Available online at www.sciencedirect.com

ScienceDirect

Ceramics International 40 (2014) 409–415

CERAMICS INTERNATIONAL

www.elsevier.com/locate/ceramint

Nanostructured TiO_2 films: Enhanced NH_3 detection at room temperature

P. Dhivya[a], Arun K. Prasad[b], M. Sridharan[a,*]

[a]*Functional Nanomaterials & Device Lab, Centre for Nanotechnology & Advanced Biomaterials and School of Electrical & Electronics Engineering, SASTRA University, Thanjavur 613401, India*

[b]*Materials Science Group, Indira Gandhi Centre for Atomic Research, Kalpakkam 603102, India*

Received 27 May 2013; received in revised form 10 June 2013; accepted 10 June 2013
Available online 24 June 2013

Abstract

The influence of substrate bias on the ammonia (NH_3) sensing properties of reactive dc magnetron sputtered titanium dioxide (TiO_2) films has been investigated. The films deposited at floating potential and −100 V substrate bias exhibited a mixed phase (anatase and rutile) as analysed by X-ray diffraction (XRD) while the films deposited at −200 V substrate bias had only rutile phase. On increasing the substrate bias voltage the grain size increased from 15 to 31 nm and the optical band gap value decreased. The TiO_2 films had an enhanced response towards NH_3 in the concentration range 5−100 ppm at room temperature. The enhanced performances are correlated to the high surface-to-bulk ratio and crystal structure. The TiO_2 film deposited at lower bias has enhanced sensitivity of (S-7857) towards NH_3 at room temperature with quick response and recovery time.

Keywords: A. Films; D. TiO_2; E. Sensors; Sensitivity

1. Introduction

Ammonia (NH_3) plays a vital role in all forms of life and it is generally produced by the way of natural process in animals, human and plants. In addition to this, NH_3 is synthesized artificially due to its variety of applications in the field of explosives production, fertilizers, pesticides, textile, food processing, household cleaning and bleaching products. Although the threshold value for NH_3 concentration in air is 25 ppm for human being, above 25 ppm concentration of NH_3 it causes irritation to the respiratory system, eyes and skin and long term exposure of NH_3 leads to fatal [1]. Hence, there is a necessity for developing cost effective, reliable NH_3 sensors to detect in lower ppm with excellent performance. Various metal oxides are being used to detect NH_3 such as ZnO [2,3], WO_3 [4,5], TiO_2 [6,7], SnO_2 [8,9], etc. Among all sensors, room temperature based ammonia sensors can offer cost-reduction because of its reduced working temperature, low power consumption of sensor, miniaturized size and improved sensor life time. TiO_2 is an inexpensive, non-toxic and wide band gap n-type semiconductor. TiO_2 has high thermal stability, photocatalytic activity, chemical stability and high corrosion resistance [10]. The superior dielectric properties of TiO_2 meets the demand in ultra large scale integration, used as an alternative dielectric to silicon dioxide [11]. These features make TiO_2 as one of the potential candidates for gas sensing application.

Different deposition techniques such as, chemical vapour deposition [12], dip coating [13], spin coating [14], spray pyrolysis [15], magnetron sputtering [16], etc., are used to deposit TiO_2 films. Among all these techniques, dc magnetron sputtering has an advantage of controlling film thickness, uniform large area coating, well adherence of the film over the substrate, allows growth of films under a reactive atmosphere and avoids contaminants in the films during the deposition process. By changing the deposition conditions like partial pressure of argon, partial pressure of oxygen, substrate bias voltage, cathode power, substrate to target distance, deposition temperature, one can tailor the properties of TiO_2 films.

In this present work, TiO_2 films has been deposited by reactive dc magnetron sputtering and the influence of substrate

*Corresponding author. Tel.: +91 4362 304000x2277; fax: +91 4362 264120.
E-mail address: m.sridharan@ece.sastra.edu (M. Sridharan).

0272-8842/$ - see front matter © 2013 Elsevier Ltd and Techna Group S.r.l. All rights reserved.
http://dx.doi.org/10.1016/j.ceramint.2013.06.016

bias on their structural, optical, morphological properties and NH_3 detection at room temperature are studied.

2. Materials and methods

2.1. Film deposition

TiO_2 films were deposited by reactive dc magnetron sputtering on to thoroughly cleaned microscopic glass substrates (1×1 cm^2). The illustrative representation of deposition chamber is shown in Fig. 1. The glass substrates were ultrasonically cleaned in acetone, isopropanol and deionized water (15 min in each solution). Subsequently, the substrates were dried in oven for 1 h. The well cleaned substrates were placed on to the substrate holder and the deposition chamber was evacuated to a base pressure of 1×10^{-5} mbar. Titanium target (99.995% purity) of 2 in. diameter and 3.2 mm thickness was used as the source. Before depositing the films the target was sputter cleaned for 30 min (in argon) in order to remove the contamination on the target surface. Argon (15 sccm) and oxygen (4 sccm) gases were introduced inside the vacuum chamber using mass flow controllers. The source to substrate distance and the cathode power were maintained as 3 cm and 100 W respectively. And all the depositions were carried out for 15 min. The films were deposited at floating potential, −100 and −200 V bias voltages at room temperature.

2.2. Characterization techniques

The crystalline properties of the films were characterized by XRD (Bruker, D8 Focus, Germany) using CuK_α radiation in the diffraction angle range of 20–40°. The surface morphology of the films was studied by using field emission scanning electron microscope (FESEM) (Carl Zeiss SUPRA55, Germany). The elemental composition of the films was determined using energy dispersive analysis of X-ray (EDAX) attached with the FESEM. The thicknesses of the films were measured using ellipsometry (Filmmetric F20, USA) and were found to be in the range of 130–200 nm. The optical properties of the films were studied by double-beam UV–vis spectroscopy (Perkin Elmer, Lambda 35, USA) in the wavelength range of 200–800 nm.

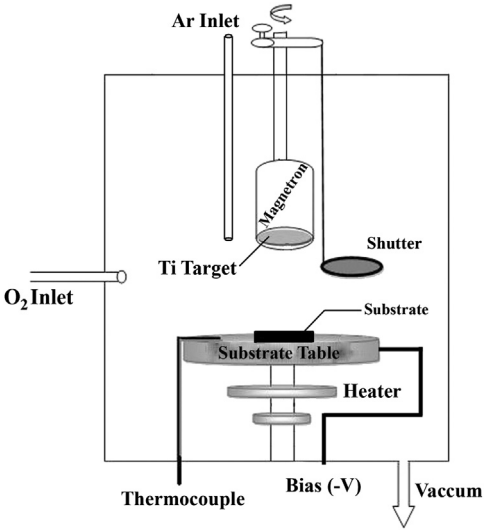

Fig. 1. Schematic representation of dc magnetron deposition setup.

2.3. Gas sensing setup

The gas sensing studies were performed in a custom built sensing setup. The schematic diagram of the gas sensing setup is shown in Fig. 2. The sensing setup consists of gas sensing chamber (volume 1 l), picoammeter (DPM-111), high voltage power supply (EHT-11) and vacuum pump (VE115N). Before injecting NH_3 inside the test chamber, the sensor with TiO_2 film as the active layer was stabilized to attain the stable baseline in ambient air. After fixing the baseline, the NH_3 was injected using a micro-syringe of required concentration. And the change in the resistance value of the TiO_2 films was constantly recorded using picoammeter.

3. Results and discussion

3.1. Structural properties

The XRD patterns of TiO_2 films deposited at floating potential, −100 and −200 V are shown in Fig. 3. The films deposited at floating potential had higher percentage of anatase phase and smaller fraction of rutile phase. The films deposited at −100 V bias consisted of smaller fraction of anatase phase and higher fraction of rutile phase of TiO_2 and with peaks corresponding to (101) and (110) planes. The films deposited at −200 V contain single phase of rutile TiO_2 with its corresponding plane at (110) and this is in concurrence with the JCPDS card no. 21-1272 [17]. The deposited film shows no other impurity peak, which suggests that the deposited films are of high purity. When increasing the bias voltage from −100 to −200 V the anatase peak (101) disappeared and large fraction of rutile phase (110) is only observed. This may be due to the fact that the anatase phase is less stable than the rutile and also substrate bias voltage increases the kinetic energy of the bombarding Ar^+ ions that creates large number of nucleation sites [18]. The crystallite size was calculated using Debye Scherrer formula [19]

$$D = k\lambda/\beta \cos\theta \quad (1)$$

where k is the shape factor, λ is the wavelength of the X-ray, β is the full-width half-maximum and θ is the diffracted angle.

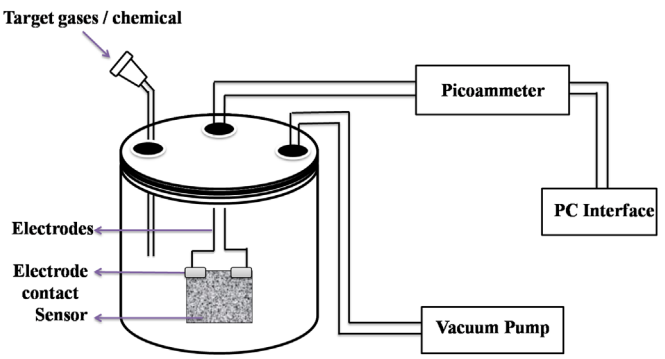

Fig. 2. Schematic diagram of gas sensing setup.

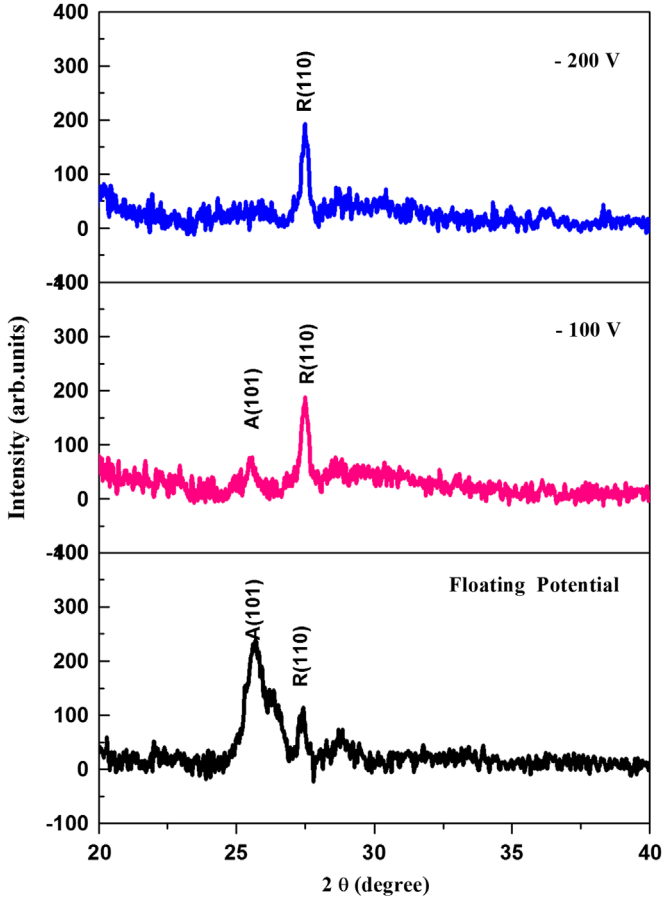

Fig. 3. XRD patterns of the TiO_2 films deposited at different bias voltages.

The crystallite size was found to be 15, 27 and 31 nm for the film deposited at floating potential, −100 and −200 V respectively.

3.2. Morphological studies

The FESEM micrographs of the TiO_2 films deposited at different bias voltages are shown in Fig. 4. The films deposited at floating potential are fairly uniform throughout the substrate with distribution of small spherical grains of size 20–25 nm. It is seen that the film deposited at −100 V consists of spherical grains and the density of smaller grains is higher than that of the larger agglomerates. The smaller agglomerates have a size of 20–30 nm. At −200 V grain size of 30–40 nm was obtained. The grain sizes of the TiO_2 films observed from FESEM micrographs were well supported with the values calculated from XRD data. EDAX spectrum shows the presence of Ti and O. Silicon (Si) peak that was detected was due to the presence of Si in glass substrate and the platinum (Pt) peak that was observed was due to the coating of the sample for FESEM analysis.

3.3. Optical properties

Optical properties of TiO_2 films deposited at different substrate bias voltage were studied using UV–visible spectrometer in the wavelength range of 200–800 nm. The optical band gap of the films were determined by Tauc's plot [20], using the following relation.

$$(\alpha h\nu)^{1/n} = A(h\nu - E_g) \quad (2)$$

where $h\nu$ is the photon energy, E_g is the optical band gap of the film, α is the absorption co-efficient. A is the constant exponent corresponding to the type of transition which occurs in the material where $n = 1/2$, 2, 3/2 and 3 corresponding to the allowed indirect, direct, forbidden indirect and forbidden direct transitions. For calculating direct band gap by using Tauc's plot, we assumed $n = 2$ for plotting the graph $(\alpha h\nu)^2$ on Y-axis and photon energy $(h\nu)$ on X-axis. By extrapolating the linear portion of the graph the intercept on the X-axis gives the direct band gap. The optical band gap was about 3.71, 3.62 and 3.51 eV for the film deposited at floating potential, −100 and −200 V respectively as shown in Fig. 5. The observed band gap values were found in concurrence with the previous report [21]. The decrease in the band gap with increasing the bias voltage is attributed to the phase transformation from anatase to rutile, which is having a lower band gap when compared to anatase. Another reason for the decrease in the band gap could be the reduction of defects in the films due to the increase of grain size [22].

3.4. NH_3 sensing studies

We have examined the NH_3 sensing characteristics of TiO_2 films at room temperature (~30 °C) in ambient atmosphere. Aluminium (Al) electrical contacts were deposited over the TiO_2 films by depositing Al (99.99% purity) using the vacuum evaporation technique [23]. Prior to exposure of NH_3, the base resistance of the TiO_2 film was stabilized in ambient atmosphere. Once, stable resistance was observed for the film, required amount of NH_3 was injected inside the sensing chamber and the resistance values were continuously recorded. The stable baselines of 1.10 and 2.00×10^{11} were observed for the films deposited at −100 and −200 V respectively. No stable resistance was observed in the case of film deposited at floating potential. So the films deposited at −100 V and −200 V bias were taken into account for further gas sensing studies.

The working principle of metal oxide based gas sensor is explained as follows. When the surface of metal oxide interacts with atmosphere, the oxygen species captures the electrons from conduction band of the metal oxide surface. Hence, the resistance of the metal oxide surface was increased in the case of n-type semiconductor and in the case of p-type semiconductor the resistance decreases. When the target gas interacts with the metal oxide surface it may donate electrons to the metal oxide surface or capture the electrons from metal oxide surface corresponding to whether it is reducing or oxidizing gas [24–26].

The interaction of oxygen species and NH_3 vapour is depicted as follows:

$$O_2(gas) \leftrightarrow O_2(ads) \quad (3)$$

$$O_2(ads) + e^- \leftrightarrow O_2^-(ads)$$

$$NH_3(gas) \leftrightarrow NH_3(ads)$$

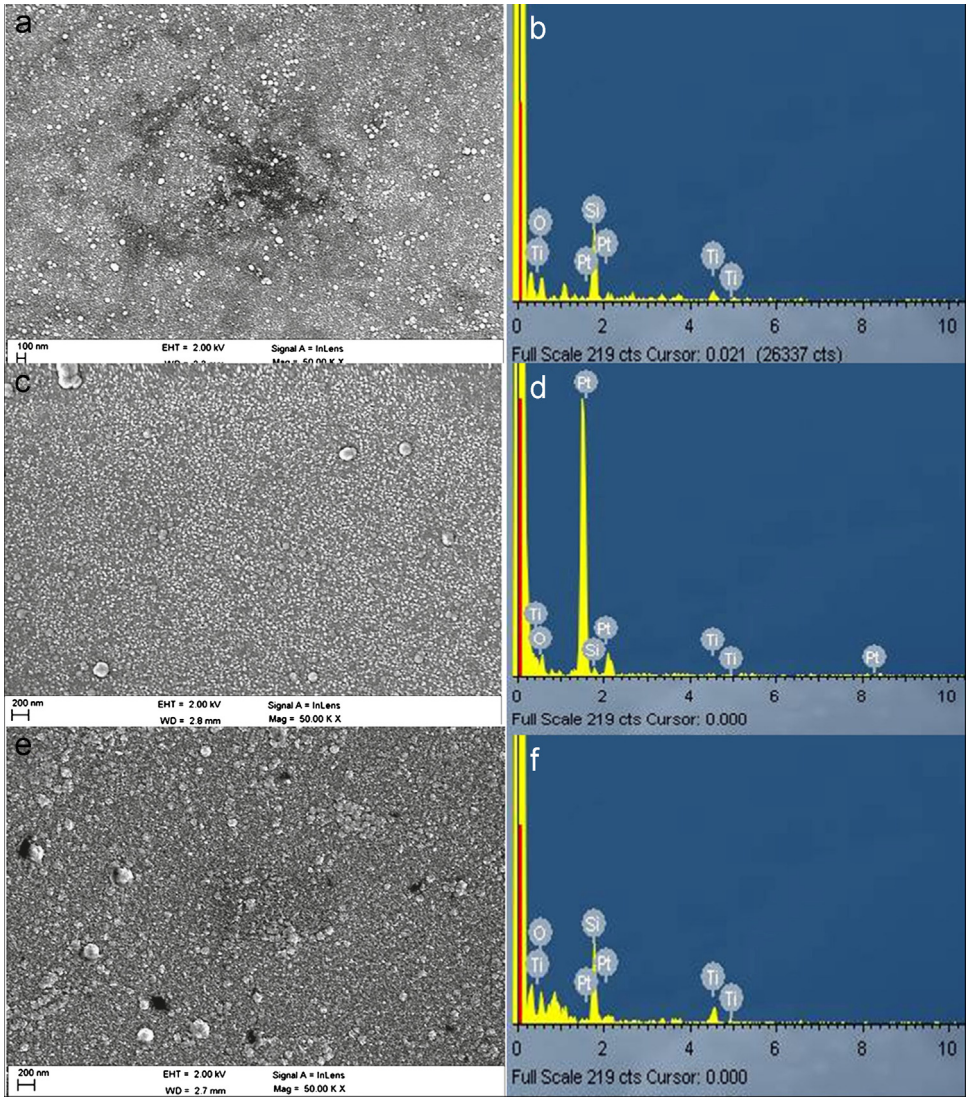

Fig. 4. FESEM micrographs (a)–(c) and EDAX patterns (d)–(f) of TiO_2 films deposited at different bias voltages.

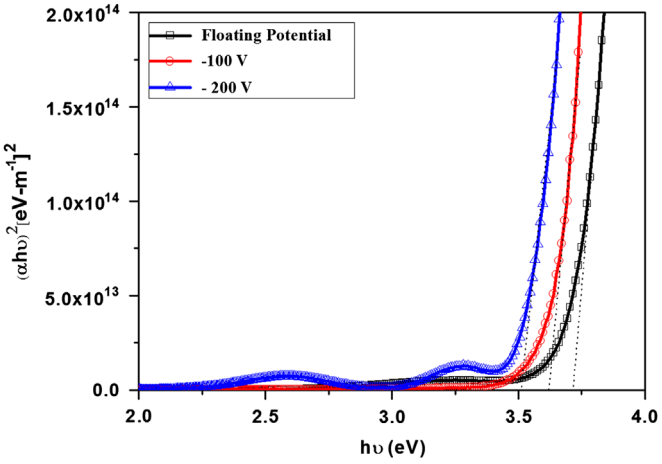

Fig. 5. Tauc's plot of TiO_2 thin films.

$$2NH_3(gas) + 5\ O^-(ads) \leftrightarrow 2NO(ads) + 3H_2O + 5e^- \quad (4)$$

The transient response of TiO_2 films deposited at −100 and −200 V substrate bias voltage towards different concentrations of NH_3 vapour are shown in Fig. 6(a) and (b). As the concentration of NH_3 increases from 5 to 100 ppm the resistance of the TiO_2 films was decreased. The magnitude of the change in the resistance of the TiO_2 films depends on the NH_3 vapour concentration. It is due to the fact that when small concentration of gas is exposed on a fixed area, resulting in lower coverage of gas on the surface leads to low response. At higher concentration, the gas molecules interacting on the surface active sites were increased, which leads to higher response of the film. The change in resistance and sensor response (S) of the TiO_2 films deposited at −100 and −200 V are presented in Table 1.

The sensor response of the film was measured using

$$S = R_a/R_g \quad (5)$$

where R_a is the resistance of the sensor in dry air condition and R_g is the resistance of the sensor in the presence of NH_3.

In case of the film deposited at −100 V, upon injecting the 100 ppm of NH_3 vapours resistance of TiO_2 films decreased rapidly by more than 5 orders of magnitude in less than a

minute. This indicates that TiO_2 films were highly sensitive ($S=7875$) to NH_3 at room temperature. But the film deposited at −200 V showed reduced sensor response ($S=1333$) as compared with the films deposited at −100 V. The higher sensitivity towards NH_3 at room temperature observed for the films deposited at −100 V, may be due to the high surface to volume ratio and also the presence of the anatase phase which has higher electron mobility [27,28]. The sensor response of the TiO_2 films is shown in Fig. 7. The sensor response of both the TiO_2 films deposited at different substrate bias voltages is comparatively higher than the values reported in the literatures [29–34], which is shown in Table 2.

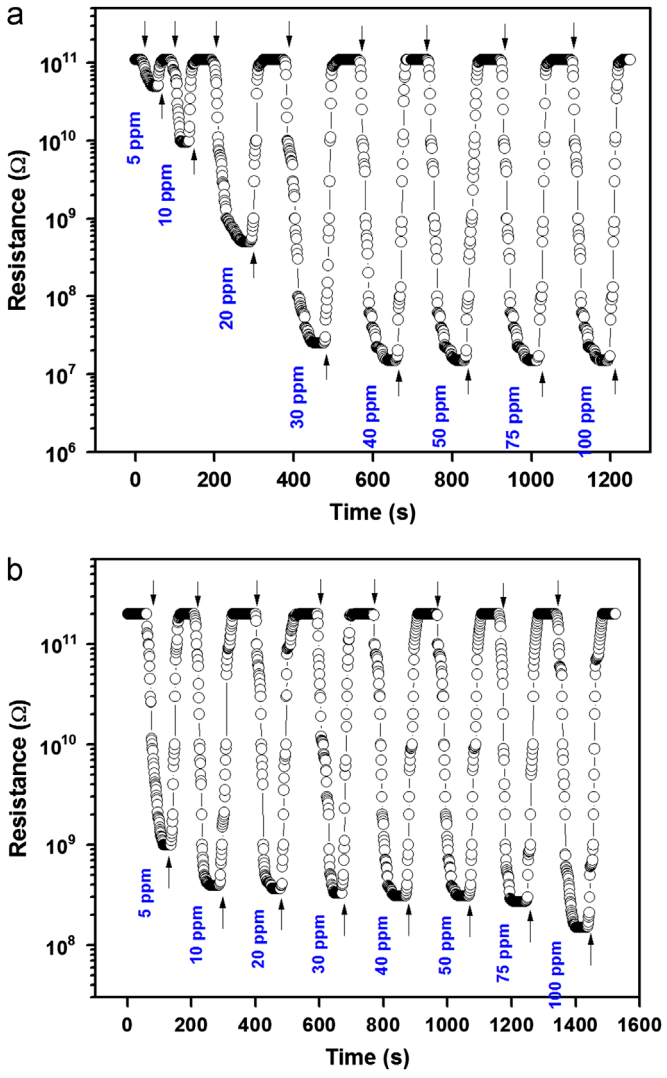

Fig. 6. Transient NH_3 sensing behaviour of TiO_2 films deposited at (a) −100 and (b) −200 V.

3.4.1. Response and recovery time

The response and recovery times of the TiO_2 films with respect to different NH_3 vapour concentrations were studied. The response and recovery time defined as time taken by the sensor output to reach 90 % of its saturation after applying or switching off the target analyte [35,36]. In our case, films have relatively faster response and recovery times of ~34–65 s 90–115 s respectively when increasing the concentration of NH_3 from 5 to 100 ppm. The slower recovery time is due to the low

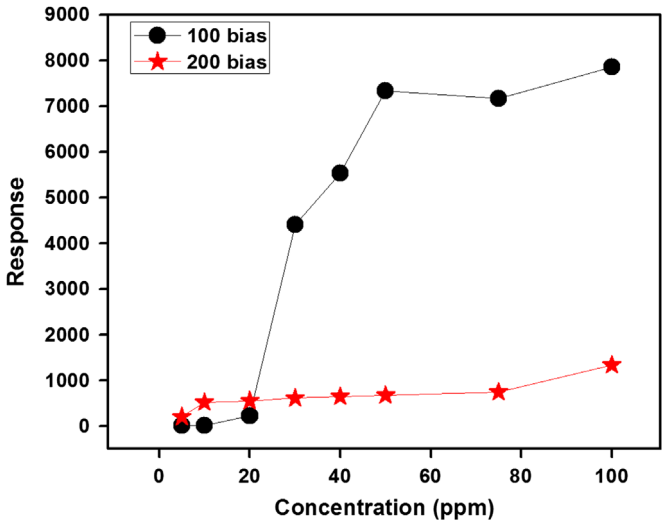

Fig. 7. Sensor response of TiO_2 thin films towards NH_3.

Table 1
Variation in resistance and response of the TiO_2 films for different NH_3 concentrations.

Gas concentration in ppm	Substrate bias voltage			
	−100 V		−200 V	
	Change in resistance (Ω)	Response	Change in resistance (Ω)	Response
0	1.10×10^{11}	–	2.00×10^{11}	–
5	5.00×10^{10}	2.2	1.00×10^{9}	200
10	9.50×10^{9}	12	3.90×10^{8}	513
20	5.00×10^{8}	220	3.65×10^{8}	548
30	2.50×10^{7}	4400	3.30×10^{8}	606
40	1.99×10^{7}	5528	3.10×10^{8}	645
50	1.50×10^{7}	7333	3.00×10^{8}	667
75	1.53×10^{7}	7171	2.70×10^{8}	741
100	1.40×10^{7}	7857	1.50×10^{8}	1333

Table 2
Comparison of TiO_2 based NH_3 sensors.

S. no	Material	Operating temperature (°C)	Detection range (ppm)	Response time (s)	Recovery time (s)	Sensor response	Ref.
1	TiO_2	250	500–5000	90	110	7000	6
2	TiO_2–polyaniline	RT	20–100	40	500	47	29
3	Cellulose–TiO_2–MWCNT	RT	50–500	100	50	50	30
4	Pt dispersed TiO_2	200	1000	–	–	100	31
5	PANi/TiO_2	RT	23–141	2	60	2	32
6	PANi/TiO_2	RT	23–141	1	58	1.67	33
7	TiO_2	200	100	20	60	11	34
8	TiO_2	**RT**	**5–100**	**34**	**90**	**7857**	**Present work**

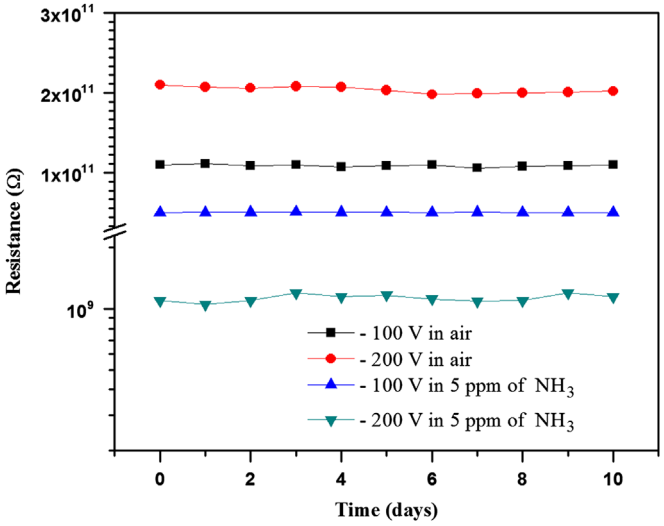

Fig. 8. Stability of the TiO_2 films towards 5 ppm NH_3.

desorption rate of the NH_3 vapour from the film surface at room temperature [37].

3.4.2. Stability

Stability is one of the most important concerns while working with room temperature sensors. Stability is defined as the ability of the sensor to provide reproducible results for certain period of time. This includes retaining the sensitivity, selectivity, response and recovery time [38]. Poor stability of sensor may lead to false alarm and leading to frequent recalibration or replacement of the sensor. The stability of TiO_2 film sensor deposited at different bias voltages is shown in Fig. 8. The TiO_2 films deposited at −100 and −200 V exhibit an excellent stability for 5 ppm of NH_3 vapour over a period of 10 days. In the period of 10 days no drift in the sensor response was observed.

4. Conclusion

Nanostructured TiO_2 films were deposited at different substrate bias voltages on to glass substrates. The deposited films were polycrystalline in nature and the phase change from anatase to rutile was observed on increasing the substrate bias voltage. The band gap value decreased from 3.71 to 3.51 eV on increasing the bias voltage. From the sensing studies it was concluded that the TiO_2 deposited at −100 V has enhanced sensor response ($S=7857$) towards NH_3 with fast response and recovery time of 34 and 90 s respectively. The TiO_2 thin films are capable to detect NH_3 as low as 5 ppm and were found to be highly stable. The simplicity, low-cost, high sensitivity and high stability of the TiO_2 films meet the requirement as a sensor for environmental monitoring.

Acknowledgements

The authors thank DRDO for the financial support and SASTRA University for providing the experimental facilities.

References

[1] B. Timmer, W. Olthuis, A.V.Den Berg, Ammonia sensors and their applications—a review, Sensors and Actuators B 107 (2005) 666–677.
[2] G.S. Rao, D. Trivikrama, Tarakarama Rao, Gas sensitivity of ZnO based thick film sensor to NH_3 at room temperature, Sensors and Actuators B 55 (1999) 166–169.
[3] N.K. Singh, S. Shrivastava, S. Rath, S. Annapoorni, Optical and room temperature sensing properties of highly oxygen deficient flower-like ZnO nanostructures, Applied Surface Science 257 (2010) 1544–1549.
[4] N.V. Hieu, V.V. Quang, N.D. Hoa, D. Kim, Preparing large-scale WO_3 nanowire-like structure for high sensitivity NH_3 gas sensor through a simple route, Current Applied Physics 11 (2011) 657–661.
[5] Y.M. Zhao, Y.Q. Zhu, Room temperature ammonia sensing properties of $W_{18}O_{49}$ nanowires, Sensors and Actuators B 137 (2009) 27–31.
[6] B. Karunagaran, P. Uthirakumar, S.J. Chung, S. Velumani, E.K. Suh, TiO_2 thin film gas sensor for monitoring ammonia, Materials Characterization 58 (2007) 680–684.
[7] M. Sánchez, M.E. Rincón, Sensor response of sol–gel multiwalled carbon nanotubes–TiO_2 composites deposited by screen-printing and dip-coating techniques, Sensors and Actuators B 140 (2009) 17–23.
[8] A. Jerger, H. Kohler, F. Becker, H.B. Keller, R. Seifert, New applications of tin oxide gas sensors: II. intelligent sensor system for reliable monitoring of ammonia leakages, Sensors and Actuators B 81 (2002) 301–307.
[9] C.W. Lin, H.I. Chen, T.Y. Chen, C.C. Huang, C.S. Hsu, R.C. Liu, W.C. Liu, On an indium-tin-oxide thin film based ammonia gas sensor, Sensors and Actuators B 160 (2011) 1481–1484.
[10] W. Zhang, W. Liu, C. Wang, Tribological behavior of sol–gel TiO_2 films on glass, Wear 253 (2002) 377–384.

[11] K. Okimura, Low temperature growth of rutile TiO_2 films in modified rf magnetron sputtering, Surface and Coatings Technology 135 (2001) 286–290.
[12] B. Vallejo, M. Gonzalez-Mañas, J. Martínez-López, F. Morales, M.A. Caballero, Characterization of TiO_2 deposited on textured silicon wafers by atmospheric pressure chemical vapour deposition, Solar Energy Materials and Solar Cells 86 (2005) 299–308.
[13] R. Mechiakh, N.B. Sedrine, J.B. Naceur, R. Chtourou, Elaboration and characterization of nanocrystalline TiO_2 thin films prepared by sol–gel dip-coating, Surface and Coatings Technology 206 (2011) 243–249.
[14] A. Elfanaoui, E. Elhamri, L. Boulkaddat, A. Ihlal, K. Bouabid, L. Laanab, A. Taleb, X. Portier, Optical and structural properties of TiO_2 thin films prepared by sol–gel spin coating, International Journal of Hydrogen Energy 36 (2011) 4130–4133.
[15] A. Conde-Gallardo, M. Guerrero, N. Castillo, A.B. Soto, R. Fragoso, G. Cabañas-Moreno, TiO_2 anatase thin films deposited by spray pyrolysis of an aerosol of titanium diisopropoxide, Thin Solid Films 473 (2005) 68–73.
[16] M.C. Liao, H. Niu, G.S. Chen, Effect of sputtering pressure and post-annealing on hydrophilicity of TiO_2 thin films deposited by reactive magnetron sputtering, Thin Solid Films 518 (2010) 7258–7262.
[17] Joint Committee on Powder Diffraction Standards (JCPDS), Powder Diffraction File, Card no. 21-1272, Swarthmore, PA.
[18] Y.C. Feng, D.E. Laughlin, D.N. Lambeth, Formation of crystallographic texture in rf sputter deposited Cr thin films, Journal of Applied Physics 76 (1994) 7311–7316.
[19] D.B. Cullity, Elements of X-ray Diffraction, Addison-Wesley Inc., Massachusetts, 1956.
[20] J. Tauc, Amorphous and Liquid Semiconductors, Plenum, London, 1974.
[21] M.M. Hasan, A.S.M.A. Haseeb, R. Saidur, H.H. Masjuki, M. Hamdi, Influence of substrate and annealing temperatures on optical properties of RF-sputtered TiO_2 thin films, Optical Materials 32 (2010) 690–695.
[22] Monjoy Sreemany, Ankita Bose, Suchitra Sen, A study on structural, optical, electrical and microstructural properties of thin TiO_x films upon thermal oxidation: effect of substrate temperature and oxidation temperature, Physica B 405 (2010) 85–93.
[23] P. Dhivya, A.K. Prasad, M. Sridharan, Nanostructured cadmium oxide thin films for hydrogen sensor, International Journal of Hydrogen Energy 37 (2012) 18575–18578.
[24] J. Tamaki, C. Naruo, Y. Yamamoto, M. Matsuoka, Sensing properties to dilute chlorine gas of indium oxide based thin film sensors prepared by electron beam evaporation, Sensors and Actuators B 83 (2002) 190–194.
[25] G. Korotcenkov, Metal oxides for solid-state gas sensors: what determines our choice?, Materials Science and Engineering B 139 (2007) 1–23
[26] G. Korotcenkov, I. Blinov, M. Ivanov, J.R. Stetter, Ozone sensors on the base of SnO_2 films deposited by spray pyrolysis, Sensors and Actuators B 120 (2007) 679–686.
[27] A. Karuppasamy, A. Subrahmanyam, Studies on the room temperature growth of nanoanatase phase TiO_2 thin films by pulsed dc magnetron with oxygen as sputter gas, Journal of Applied Physics 101 (2007) 064318-7.
[28] Ibrahim A. Al-Homoudi, J.S. Thakur, R. Naik, G.W. Auner, G. Newaz, Anatase TiO_2 films based CO gas sensor: film thickness, substrate and temperature effects, Journal of Applied Physics 253 (2007) 8607–8614.
[29] S.G. Pawar, M.A. Chougule, S.L. Patil, B.T. Raut, P.R. Godse, Shashwati Sen, V.B. Patil, Room temperature ammonia gas sensor based on polyaniline–TiO_2 nanocomposite, IEEE Sensors 11 (2011) 3417–3423.
[30] S. Mun, Y. Chen, J. Kim, Cellulose–titanium dioxide–multiwalled carbon nanotube hybrid nanocomposite and its ammonia gas sensing properties at room temperature, Sensors and Actuators B 171–172 (2012) 1186–1191.
[31] I. Hayakawa, Y. Iwamoto, K. Kikuta, S. Hirano, Gas sensing properties of metal-organics derived Pt dispersed-TiO_2 thin film fired in NH_3, Sensors and Actuators B 67 (2000) 270–274.
[32] H. Tai, Y. Jiang, G. Xie, J. Yu, X. Chen, Z. Ying, Influence of polymerization temperature on NH_3 response of PANI/TiO_2 thin film gas sensor, Sensors and Actuators B 129 (2008) 319–326.
[33] H. Tai, Y. Jiang, G. Xie, J. Yu, X. Chen, Fabrication and gas sensitivity of polyaniline–titanium dioxide nanocomposite thin film, Sensors and Actuators B 125 (2007) 644–650.
[34] Shailesh Pawar, Manik Chougule, Sanjay Patil, Bharat Raut, Dhanaji Dalvi, Pramod Patil, P.J. Shashwati Sen, Vikas Patil, Fabrication of nanocrystalline TiO_2 thin film ammonia vapor sensor, Journal of Sensor Technology 1 (2011) 9–16.
[35] Xing-Jiu Huang, Yang-Kyu Choi, Chemical sensors based on nanostructured materials, Sensors and Actuators B 122 (2007) 659–671.
[36] I. Lundström, Approaches and mechanisms to solid state based sensing, Sensors and Actuators B 35 (1996) 11–19.
[37] A. Šetkus, A. Galdikas, A. Mironas, V. Strazdien, I. Šimkien, I. Ancutien, V. Janickis, S. Kačiulis, G. Mattogno, G.M. Ingo, The room temperature ammonia sensor based on improved Cu_xS-micro-porous-Si structure, Sensors and Actuators B 78 (2001) 208–215.
[38] Marion E. Franke, Tobias J. Koplin, Ulrich Simon, Metal and metal oxide nanoparticles in chemiresistors: does the nanoscale matter?, Small 2 (2006) 36–50.